Electronic Supplementary Material (ESI) for ChemComm.
This journal is © The Royal Society of Chemistry 2023

Electronic Supplementary Information

Unveiling Light Effect on Formation of Trisulfur Radicals in Lithium–Sulfur Batteries

Bohai Zhang,[a, b] Zhenyu Wang,[c] Huifu Ji,[a] Hao Zhang,[a] Lanlan Li,[a] Jiandong Hu,[a] Shixin Li,[a] and Junfeng Wu*[, a]

[a.] *Henan International Joint Laboratory of Laser Technology in Agriculture Sciences, College of Mechanical & Electrical Engineering, Henan Agricultural University, Zhengzhou 450002, Henan, China.*

[b.] *Institute of New Energy Material Chemistry, School of Materials Science and Engineering, Nankai University, Tianjin 300350, China.*

[c.] *Institute of Science and Technology, China Three Gorges Corporation, Beijing 101100, China.*

**Corresponding author. E-mail: jfwu@henau.edu.cn*

S1 Experimental and calculation

S1.1 Preparation of the Li_2S_6 solution and the electrolyte with Li_2S_6

Li_2S_6 solution was prepared by mixing Li_2S and S with a stoichiometric ratio of 1:5 into DMSO solvent, *i.e.*, $Li_2S + 5S = Li_2S_6$. The prepared solution was then diluted to the concentration of interest. The electrolyte used in this work was prepared by dissolving 1.0 M lithium bis(trifluoromethanesulfonyl)imide (LiTFSI) in DMSO, which was set as the blank electrolyte. The electrolyte which contains Li_2S_6 was prepared by diluting Li_2S_6 solution in the blank electrolyte.

S1.2 Spectroscopic characterization

Raman spectroscopy was measured on a Raman spectrometer (SR-500I-A) with a 532 nm laser. UV-vis spectra were measured on a UV-vis spectrophotometer (CARY 100 Cone), with deuterium (200 − 350 nm) and tungsten (350 − 800 nm) lamps as the light source. All ESR measurements were tested on an ESR spectrometer (MS400) under dark conditions, with a microwave frequency of ~9.3 GHz at the power of 20 mW power. The sweeping rate was set at 7.19 GHz/s. SEM images were performed using a field emission scanning electron microscope (JSM-7800) with an elemental mapping apparatus.

S1.3 Electrochemical Measurements

The graphene/sulfur (G/S) composite was synthesized through the melting method. In this method, graphene and sulfur were mixed at 1:3 ratio and heated to 155 °C. The sulfur cathode consists of an 80 wt% of G/S composite, 10 wt% of Super-P conductive carbon, and 10 wt% of PVDF binder. The areal sulfur loading of cathodes is ca. 1.0 mg cm^{-2} and E/S = 10 μL mg^{-1}. Li−S cells were assembled in an Ar-filled glovebox using Celgard 2300 separator and Li metal anode. Galvanostatic discharge and charge tests were performed at 0.1 C (1 C = 1675 mA g^{-1}) on a LAND battery test system (CT2001C) within the potential range of 1.7 − 2.8 V (*vs*. Li/Li^+). Electrochemical impedance spectra (EIS) were performed on an electrochemical workstation (ZAHNER elektrik IM6ex) from 100 kHz to 10 mHz, with an amplitude of 5 mV. The specific capacity of Li−S cells was calculated based on the mass of total sulfur, including sulfur of Li_2S_6.

S1.4 *Ab initio* calculations

The geometrical optimizations of Li^+-DMSO and polysulfide-DMSO clusters were calculated by *ab initio* calculations in the gas phase. The density functional was selected as M06-2X,[1] with the basis set of 6-31+G(d). The D3 dispersion correction was selected to present the weak interaction in the clusters. The optimized configurations were subjected to frequency calculations to ensure that they were at a local minimum of the potential energy surface. The Gibbs free energy correction at P° = 1 atm and T = 298.15 K was obtained by canonical

ensemble partition function. The cluster-continuum solvation model[2] was utilized to obtain $\Delta G^*(\mathrm{X})$, where ($\mathrm{X} = \mathrm{Li}^+, \mathrm{Li_2S_6}, \mathrm{LiS_6^-}, \mathrm{S_6^{2-}}, \mathrm{LiS_4^\bullet}, \mathrm{LiS_3^\bullet}, \mathrm{LiS_2^\bullet}, \mathrm{S_4^{\bullet-}}, \mathrm{S_3^{\bullet-}}$, and $\mathrm{S_2^{\bullet-}}$). The solvation Gibbs free energies of Li^+-DMSO and polysulfide-DMSO clusters were calculated by SMD solvation model.[3]

The calculated Raman spectra were obtained at M06-2X/6-31+G(d)[1] level of theory with the SMD solvation model.[3] The calculated UV-vis spectra were obtained by TD-DFT[4] calculations at M06-2X/6-311+G(2d,p) level of theory with the SMD solvation model, based on the benchmark study by Truhlar *et al.*[5]

Vertical electron affinity (VEA) and nucleophilicity index (NI) of X species ($\mathrm{X} = \mathrm{Li_2S_6}, \mathrm{LiS_6^-}, \mathrm{S_6^{2-}}, \mathrm{LiS_3^\bullet}$, and $\mathrm{S_3^{\bullet-}}$) were calculated by M06-2X/6-31+G(d) level of theory with SMD solvation model. $\mathrm{VEA(X)} = E_N(\mathrm{X}) - E_{N+1}(\mathrm{X})$, in which E is the electronic energy, and N and N+1 are the electron states. $\mathrm{NI} = E_{\mathrm{HOMO}}(\mathrm{X}) - E_{\mathrm{HOMO}}(\mathrm{TCE})$, in which TCE denotes the tetracyanoethylene molecules. The HOMO energy of tetracyanoethylene is almost the lowest among all organic molecules, and thus, it is commonly selected as a reference in NI calculation.[6] All the energy calculations mentioned above were calculated at M06-2X/6-31+G(d) level of theory, on Gaussian 16 program.[7]

S2 Calculation of dissociation constant pK_{di} (i = 1-10)

S2.1 Dissociation Gibbs free energies ΔG^*_{di} (i = 1-10)

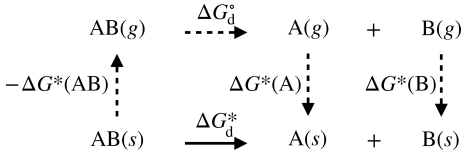

Fig. S1. The thermodynamic cycle used to calculate the ΔG^*_{di} (i = 1-10) of Rxns 1-10. AB(s) compounds can dissociate into A(s) and B(s) in the solution phase with dissociation Gibbs free energy of ΔG^*_{d}. To obtain ΔG^*_{d} for the dissociation of AB, we need to vaporize AB(s) into the gas phase (denoted as AB(g)). The negative solvation Gibbs free energy in the gas phase is $-\Delta G^*(\mathrm{AB})$. AB(g) may then dissociate into A(g) and B(g) in the gas phase with dissociation Gibbs free energy of $\Delta G^\circ_{\mathrm{d}}$. Then A($g$) and B($g$) will be solvated into the solution with solvation Gibbs free energy of $\Delta G^*(\mathrm{A})$ and $\Delta G^*(\mathrm{B})$, respectively. Finally, the calculation of Gibbs free energy of the dissociation reactions can be calculated using the following equation: $\Delta G^*_{\mathrm{d}} = \Delta G^\circ_{\mathrm{d}} + \Delta G^*(\mathrm{A}) + \Delta G^*(\mathrm{B}) - \Delta G^*(\mathrm{AB}) + 1.89$, where 1.89 is the difference of free energy between the standard state in the solution phase and gas phase. The unit is in kcal mol^{-1}.

As mentioned in the main text, there are 10 potential dissociate routes for $\mathrm{Li_2S_6}$ in DMSO solution, which can be written as follows:

$$\mathrm{Li_2S_6(s) \rightleftharpoons Li^+(s) + LiS_6^-(s)} \quad \text{(Rxn. 1)}$$

$$\mathrm{LiS_6^-(s) \rightleftharpoons Li^+(s) + S_6^{2-}(s)} \quad \text{(Rxn. 2)}$$

$$\mathrm{S_6^{2-}(s) \rightleftharpoons 2S_3^{\bullet-}(s)} \quad \text{(Rxn. 3)}$$

$$\mathrm{LiS_6^-(s) \rightleftharpoons LiS_3^\bullet(s) + S_3^{\bullet-}(s)} \quad \text{(Rxn. 4)}$$

$$\mathrm{LiS_3^{\bullet}(s) \rightleftharpoons Li^+(s) + S_3^{\bullet -}(s)} \quad \text{(Rxn. 5)}$$
$$\mathrm{S_6^{2-}(s) \rightleftharpoons S_4^{\bullet -}(s) + S_2^{\bullet -}(s)} \quad \text{(Rxn. 6)}$$
$$\mathrm{Li_2S_6(s) \rightleftharpoons 2LiS_3^{\bullet}(s)} \quad \text{(Rxn. 7)}$$
$$\mathrm{Li_2S_6(s) \rightleftharpoons LiS_4^{\bullet}(s) + LiS_2^{\bullet}(s)} \quad \text{(Rxn. 8)}$$
$$\mathrm{LiS_4^{\bullet}(s) \rightleftharpoons Li^+(s) + S_4^{\bullet -}(s)} \quad \text{(Rxn. 9)}$$
$$\mathrm{LiS_2^{\bullet}(s) \rightleftharpoons Li^+(s) + S_2^{\bullet -}(s)} \quad \text{(Rxn. 10)}$$

The Gibbs free energies for the dissociation reactions Rxns. 1-10 (ΔG^*_{di}, i = 1-10) were calculated by design thermodynamic cycle (Fig. S1). The reactants AB(s) (AB = $\mathrm{Li_2S_6}$, $\mathrm{LiS_6^-}$, $\mathrm{S_6^{2-}}$, $\mathrm{LiS_4^{\bullet}}$, $\mathrm{LiS_3^{\bullet}}$, and $\mathrm{LiS_2^{\bullet}}$) may dissociate into A(s) and B(s) (A = $\mathrm{Li^+}$, $\mathrm{LiS_4^{\bullet}}$, $\mathrm{LiS_3^{\bullet}}$, $\mathrm{S_4^{\bullet -}}$, and $\mathrm{S_3^{\bullet -}}$; B = $\mathrm{LiS_6^-}$, $\mathrm{S_6^{2-}}$, $\mathrm{LiS_3^{\bullet}}$, $\mathrm{LiS_2^{\bullet}}$, $\mathrm{S_4^{\bullet -}}$, $\mathrm{S_3^{\bullet -}}$, and $\mathrm{S_2^{\bullet -}}$) in DMSO, with dissociation Gibbs free energy of ΔG^*_{di} (i = 1-10). To obtain ΔG^*_{di} above, firstly, the dissociation Gibbs free energy ($\Delta G^\circ_{\mathrm{di}}$) of Rxns 1-10 in the gas phase were directly calculated by *ab initio* calculations at M06-2X/6-31+G(d) level of theory[1]. Then, the negative solvation Gibbs free energy of AB(s) ($-\Delta G^*(\mathrm{AB})$), and the solvation Gibbs free energy of A(s) and B(s) ($\Delta G^*(\mathrm{A})$ and $\Delta G^*(\mathrm{B})$) were calculated by the cluster-continuum model[2] at M06-2X/6-31+G(d) level of theory[1], where SMD solvation model[3] was also used. Finally, the $\Delta G^*_{\mathrm{di}} = \Delta G^\circ_{\mathrm{di}} + \Delta G^*(\mathrm{A}) + \Delta G^*(\mathrm{B}) - \Delta G^*(\mathrm{AB}) + 1.89$ was used to obtain the ΔG^*_{di} where 1.89 is the difference of Gibbs free energy between the standard state of solution phase and gas phase. The unit is in kcal $\mathrm{mol^{-1}}$. Then the ΔG^*_{di} of Rxns. 1-10 can be calculated by Eqs. S1-S10, *i.e.*,

$$\Delta G^*_{\mathrm{d1}} = \Delta G^\circ_{\mathrm{d1}} + \Delta G^*(\mathrm{Li^+}) + \Delta G^*(\mathrm{LiS_6^-}) - \Delta G^*(\mathrm{Li_2S_6}) + 1.89 \quad \text{(S1)}$$
$$\Delta G^*_{\mathrm{d2}} = \Delta G^\circ_{\mathrm{d2}} + \Delta G^*(\mathrm{Li^+}) + \Delta G^*(\mathrm{S_6^{2-}}) - \Delta G^*(\mathrm{LiS_6^-}) + 1.89 \quad \text{(S2)}$$
$$\Delta G^*_{\mathrm{d3}} = \Delta G^\circ_{\mathrm{d3}} + 2\Delta G^*(\mathrm{S_3^{\bullet -}}) - \Delta G^*(\mathrm{S_6^{2-}}) + 1.89 \quad \text{(S3)}$$
$$\Delta G^*_{\mathrm{d4}} = \Delta G^\circ_{\mathrm{d4}} + \Delta G^*(\mathrm{LiS_3^{\bullet}}) + \Delta G^*(\mathrm{S_3^{\bullet -}}) - \Delta G^*(\mathrm{LiS_6^-}) + 1.89 \quad \text{(S4)}$$
$$\Delta G^*_{\mathrm{d5}} = \Delta G^\circ_{\mathrm{d5}} + \Delta G^*(\mathrm{Li^+}) + \Delta G^*(\mathrm{S_3^{\bullet -}}) - \Delta G^*(\mathrm{LiS_3^{\bullet}}) + 1.89 \quad \text{(S5)}$$
$$\Delta G^*_{\mathrm{d6}} = \Delta G^\circ_{\mathrm{d6}} + \Delta G^*(\mathrm{S_4^{\bullet -}}) + \Delta G^*(\mathrm{S_2^{\bullet -}}) - \Delta G^*(\mathrm{S_6^{2-}}) + 1.89 \quad \text{(S6)}$$
$$\Delta G^*_{\mathrm{d7}} = \Delta G^\circ_{\mathrm{d7}} + 2\Delta G^*(\mathrm{LiS_3^{\bullet}}) - \Delta G^*(\mathrm{Li_2S_6}) + 1.89 \quad \text{(S7)}$$
$$\Delta G^*_{\mathrm{d8}} = \Delta G^\circ_{\mathrm{d8}} + \Delta G^*(\mathrm{LiS_4^{\bullet}}) + \Delta G^*(\mathrm{LiS_2^{\bullet}}) - \Delta G^*(\mathrm{Li_2S_6}) + 1.89 \quad \text{(S8)}$$
$$\Delta G^*_{\mathrm{d9}} = \Delta G^\circ_{\mathrm{d9}} + \Delta G^*(\mathrm{Li^+}) + \Delta G^*(\mathrm{S_4^{\bullet -}}) - \Delta G^*(\mathrm{LiS_4^{\bullet}}) + 1.89 \quad \text{(S9)}$$
$$\Delta G^*_{\mathrm{d10}} = \Delta G^\circ_{\mathrm{d10}} + \Delta G^*(\mathrm{Li^+}) + \Delta G^*(\mathrm{S_2^{\bullet -}}) - \Delta G^*(\mathrm{LiS_2^{\bullet}}) + 1.89 \quad \text{(S10)}$$

S2.2 Thermodynamic cycle for the calculation of $\Delta G^*(\mathrm{X})$ ($\mathrm{X = Li^+\ Li_2S_6}$, $\mathrm{LiS_6^-}$, $\mathrm{S_6^{2-}}$, $\mathrm{S_4^{\bullet -}}$, $\mathrm{S_3^{\bullet -}}$, $\mathrm{S_2^{\bullet -}}$, $\mathrm{LiS_4^{\bullet}}$, $\mathrm{LiS_3^{\bullet}}$, and $\mathrm{LiS_2^{\bullet}}$) by cluster-continuum solvation model

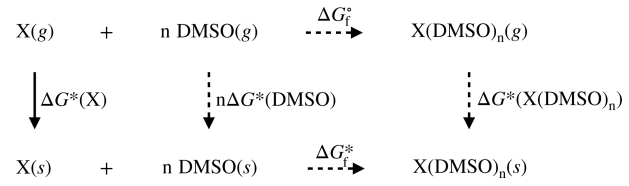

Fig. S2. Thermodynamic cycle for the calculation of solvation Gibbs free energy $\Delta G^*(\mathrm{X})$ (X = $\mathrm{Li^+}$ $\mathrm{Li_2S_6}$, $\mathrm{LiS_6^-}$, $\mathrm{S_6^{2-}}$, $\mathrm{S_4^{\bullet -}}$, $\mathrm{S_3^{\bullet -}}$, $\mathrm{S_2^{\bullet -}}$, $\mathrm{LiS_4^{\bullet}}$, $\mathrm{LiS_3^{\bullet}}$, and $\mathrm{LiS_2^{\bullet}}$) by cluster-continuum solvation model. (*s*) and (*d*) denote the solution phase and the gas phase, respectively.

To obtain the ΔG^*_{di} of Rxns. S1-S10 by Eqs. S1'-S10', the solvation Gibbs free energy $\Delta G^*(\mathrm{X})$ (X = $\mathrm{Li_2S_6}$, $\mathrm{LiS_6^-}$, $\mathrm{S_6^{2-}}$, $\mathrm{S_4^{\bullet-}}$, $\mathrm{S_3^{\bullet-}}$, $\mathrm{S_2^{\bullet-}}$, $\mathrm{LiS_4^{\bullet}}$, $\mathrm{LiS_3^{\bullet}}$, $\mathrm{LiS_2^{\bullet}}$, and $\mathrm{Li^+}$) in DMSO solution is calculated by cluster-continuum solvation model. As shown in Fig. S2, $\Delta G^*(\mathrm{X})$ in DMSO solution phase can be calculated by

$$\Delta G^*(\mathrm{X}) = \Delta G_{\mathrm{f}}^{\circ} + \Delta G^*(\mathrm{X(DMSO)_n}) - \mathrm{n}\Delta G^*(\mathrm{DMSO}) - \Delta G_{\mathrm{f}}^* - 1.89\mathrm{n} \quad \text{(S11)}$$

in which $\Delta G_{\mathrm{f}}^{\circ}$ is the formation Gibbs free energy of $\mathrm{X(DMSO)_n}$ cluster in the gas phase, followed by the solvation Gibbs free energy of $\mathrm{X(DMSO)_n}$, calculated by SMD solvation model.[3] The superscript $*$ refers to the standard state in the solution phase of concentration 1.0 M of DMSO or $\mathrm{X(DMSO)_n}$ and temperature T = 298.15 K, which can be converted to standard state (°) in the gas phase of P =1 atm and T = 298.15 K by adding $RT\ln\frac{RT}{P}$ = 1.89 kcal mol^{-1}, in which R = 0.001987 kcal mol^{-1} K^{-1} is the ideal gas constant. ΔG_{f}^* is the formation Gibbs free energy of $\mathrm{X(DMSO)_n}$ cluster in the solution phase, which can be obtained by Eq. S12, *i.e.*,

$$\Delta G_{\mathrm{f}}^* = -RT\ln\frac{[\mathrm{X(DMSO)_n}]}{[\mathrm{X}][\mathrm{DMSO}]^{\mathrm{n}}} \quad \text{(S12)}$$

in which the square bracket denotes the concentration. Since $[\mathrm{X(DMSO)_n}] = [\mathrm{X}]$, Eq. S12 can be rewritten as

$$\Delta G_{\mathrm{f}}^* = \mathrm{n}RT\ln[\mathrm{DMSO}] \quad \text{(S13)}$$

Bring Eq. S13 into Eq. S11, we have

$$\Delta G^*(\mathrm{X}) = \Delta G_{\mathrm{f}}^{\circ} + \Delta G^*(\mathrm{X(DMSO)_n}) - \mathrm{n}\Delta G^*(\mathrm{DMSO}) - \mathrm{n}RT\ln[\mathrm{DMSO}] - 1.89\mathrm{n} \quad \text{(S14)}$$

The vaporization Gibbs free energy of DMSO is

$$\Delta G_{\mathrm{vap}}(\mathrm{DMSO}) = -\Delta G^*(\mathrm{DMSO}) - RT\ln[\mathrm{DMSO}] - 1.89 \quad \text{(S15)}$$

in which $\Delta G^*(\mathrm{DMSO})$ = −8.76 kcal mol^{-1} is the self-solvation Gibbs free energy of DMSO, calculated by SMD solvation model,[3] and [DMSO] = 14.09 mol L^{-1} is the experimental molar concentration of DMSO.[8] Combining Eqs. S14 and S15, we have

$$\Delta G^*(\mathrm{X}) = \Delta G_{\mathrm{f}}^{\circ} + \Delta G^*(\mathrm{X(DMSO)_n}) + \mathrm{n}\Delta G_{\mathrm{vap}}(\mathrm{DMSO}) \quad \text{(S16)}$$

Fig. S3 depicts the optimised $\mathrm{X(DMSO)_n}$ (X = $\mathrm{Li^+}$, $\mathrm{Li_2S_6}$, $\mathrm{LiS_6^-}$, $\mathrm{S_6^{2-}}$, $\mathrm{LiS_4^{\bullet}}$, $\mathrm{LiS_3^{\bullet}}$, $\mathrm{LiS_2^{\bullet}}$, $\mathrm{S_4^{\bullet-}}$, $\mathrm{S_3^{\bullet-}}$, and $\mathrm{S_2^{\bullet-}}$) clusters in the gas phase, calculated by M06-2X/6-31+G(d) level of theory[9] with D3 dispersion correction.[10] The coordination number of $\mathrm{Li^+}$ is 4, contributed by the four oxygen atoms from four DMSO molecules, to form $\mathrm{Li^+(DMSO)_4}$ cluster, which accords with the coordination number reported in a previous study.[11] For the LiPS clusters, since $\mathrm{Li^+}$ has been coordinated/bonded by two terminal sulfur atoms, we supplemented 4 DMSO molecules to coordinate with $\mathrm{Li_2S_6}$ to form $\mathrm{Li_2S_6(DMSO)_4}$, and 2 DMSO molecules to coordinate with $\mathrm{LiS_6^-}$, $\mathrm{LiS_4^{\bullet}}$, $\mathrm{LiS_3^{\bullet}}$, and $\mathrm{LiS_2^{\bullet}}$, to form $\mathrm{LiS_6^-(DMSO)_2}$, $\mathrm{LiS_4^{\bullet}(DMSO)_2}$, $\mathrm{LiS_3^{\bullet}(DMSO)_2}$, and $\mathrm{LiS_2^{\bullet}(DMSO)_2}$, respectively. Thus, each $\mathrm{Li^+}$ will retain its 4-coordination number, either with the S-atom in LiPSs or with the O-atom from DMSO. In addition, we also assigned two DMSO molecules to coordinate with anions: $\mathrm{S_6^{2-}}$, $\mathrm{S_4^{\bullet-}}$, $\mathrm{S_3^{\bullet-}}$, and $\mathrm{S_2^{\bullet-}}$, to form $\mathrm{S_6^{2-}(DMSO)_2}$, $\mathrm{S_4^{\bullet-}(DMSO)_2}$, $\mathrm{S_3^{\bullet-}(DMSO)_2}$, and $\mathrm{S_2^{\bullet-}(DMSO)_2}$, in order to avoid

the electrons of polysulfide (radical) anions being over-polarized by continuum dielectric.[3]

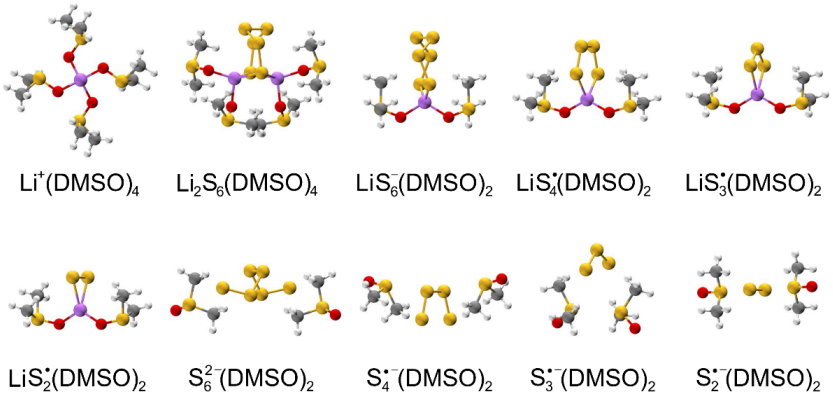

Fig. S3 The optimized X(DMSO)n (X = Li^+, Li_2S_6, LiS_6^-, S_6^{2-}, $LiS_4^\bullet$, $LiS_3^\bullet$, $LiS_2^\bullet$, $S_4^{\bullet-}$, $S_3^{\bullet-}$, and $S_2^{\bullet-}$) in the gas phase, the yellow, white, gray, red, and purple balls denote sulfur, hydrogen, carbon, oxygen, and lithium atoms, respectively.

Table S1 lists the ΔG_f°, $\Delta G^*(X(DMSO)_n)$, $n\Delta G_{vap}(DMSO)$, and $\Delta G^*(X)$ corresponding to Eq. S16.The solvation Gibbs free energy of Li^+, $\Delta G^*(Li^+)$, is –137.3 kcal·mol^{-1} in DMSO, which is in accord with that of –135.5 kcal mol^{-1} reported by Pliego *et al.*[11] Notably, $\Delta G^*(S_6^{2-})$ = –154.1 kcal mol^{-1} is the lowest solvation Gibbs free energy among all the polysulfide species studied in this work, suggesting that S_6^{2-} is the most stable species in DMSO. The dissociation Gibbs free energy ΔG_{di}^* (i = 1-10), according to Rxns. 1-10, can be calculated via $\Delta G^*(X)$ in Table S2, with the help of the Eqs. S1-S10 in S2.1.

Table S1. ΔG_f°, $\Delta G^*(X(DMSO)_n)$, $n\Delta G_{vap}(DMSO)$, and $\Delta G^*(X)$ in kcal mol^{-1} corresponding to Eq. S16

X	Li^+	Li_2S_6	LiS_6^-	S_6^{2-}	$LiS_4^\bullet$	$LiS_3^\bullet$	$LiS_2^\bullet$	$S_4^{\bullet-}$	$S_3^{\bullet-}$	$S_2^{\bullet-}$
$\Delta G^\circ(X(DMSO)_n)$	-117.0	-54.8	-15.1	-24.9	-30.9	-32.6	-33.9	-7.4	-9.1	-14.9
$\Delta G^*(X(DMSO)_n)$	-41.5	-19.6	-52.8	-139.8	-15.5	-15.1	-16.1	-46.1	-46.8	-46.2
$n\Delta G_{vap}(DMSO)$	21.2	21.2	10.6	10.6	10.6	10.6	10.6	10.6	10.6	10.6
$\Delta G^*(X)$	-137.3	-53.1	-57.3	-154.1	-35.8	-37.1	-39.4	-42.9	-45.3	-50.5

Table S2. Gibbs free energies (kcal mol^{-1}) of Rxns. 1-10 in the gas phase (ΔG_{di}°) and the DMSO solution phase (ΔG_{di}^*) and corresponding dissociation constants.

i	1	2	3	4	5	6	7	8	9	10
ΔG_{di}°	129.90	227.75	-59.05	32.47	136.23	-42.93	26.15	37.65	135.76	171.30
ΔG_{di}^*	-9.71	-4.46	6.34	9.26	-7.38	19.66	6.94	17.44	-6.75	-5.21
pK_{di}	-7.11	-3.27	4.65	6.79	-5.41	14.41	5.09	12.78	-4.94	-3.82

S2.3 Dissociation constant pK_{di} (i = 1-10)

The dissociation constant pK_{di} (i = 1-10) can be calculated by the following Eq. S17.

$$\mathrm{p}K_{\mathrm{di}} = \frac{\Delta G^{*}_{\mathrm{di}}}{2.303RT} \qquad \text{(S17)}$$

in which R = 0.001987 kcal mol^{-1} K^{-1} is the ideal gas constant, and temperature T = 298.15 K. The corresponding pK_{di} are listed in Table S2.

S3 UV-vis spectrum of pure DMSO

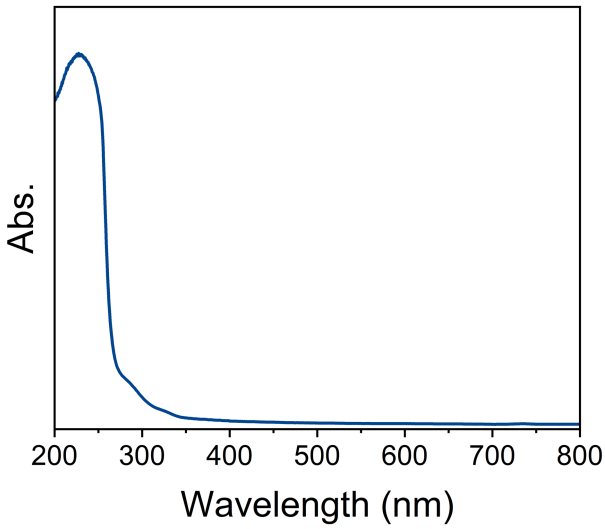

Fig. S4 UV-vis spectrum of DMSO without Li_2S_6.

S4 Calculated UV-vis spectra and natural transition orbital (NTO) pairs of S_6^{2-} and $S_3^{\bullet-}$

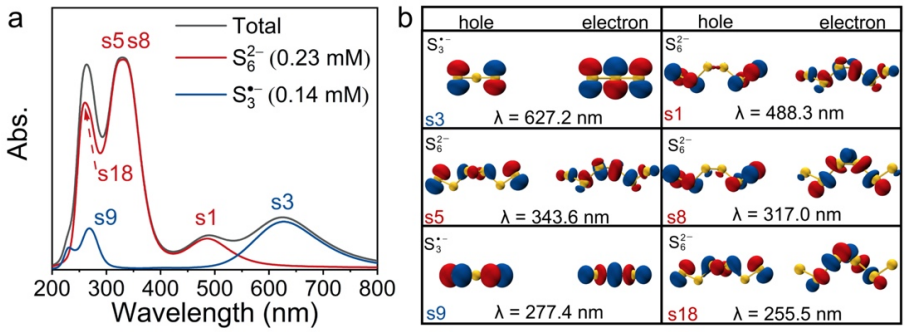

Fig. S5 (a) The calculated UV-vis spectra by TD-DFT[4] calculation at SMD/M06-2X/6-311+G(2d,p) level of theory. The red and blue curves represent the individual adsorption of S_6^{2-} and $S_3^{\bullet-}$, respectively, according to the calculated concentration of S_6^{2-} and $S_3^{\bullet-}$ using pK_{d3} in **Table S2**. The black curve represents the total adsorption weighted by the contributions of S_6^{2-} and $S_3^{\bullet-}$. (b) The NTO pairs of $S_6^{2-}$and $S_3^{\bullet-}$ which resulted in the four absorption bands seen in (a). The excitation state of each NTO pair is shown in the left corner.

The calculated UV-vis spectrum of $S_6^{2-}$and $S_3^{\bullet-}$, obtained from their calculated concentrations of 0.23 mM and 0.14 mM from pK_{d3} in Table S2, are shown in Fig. S3a. It can be seen that the calculated spectrum is consistent with the experiment in terms of peak positions. Specifically, the experimental absorption bands at 355 and 491 nm (*vs*.

332.4 and 488.3 nm by calculation) are attributed to S_6^{2-}. The absorption band at 617 nm (*vs*. 627.2 nm by calculation) is attributed to $S_3^{\bullet-}$. The absorption band at 267nm (*vs*. 261.4 nm by calculation) is attributed to the contribution of both S_6^{2-} and $S_3^{\bullet-}$. Fig. S3b illustrates the excitation model of the four absorption bands at 267, 355, 491, and 617 nm, represented by natural transition orbitals (NTOs)[12]. The two absorption bands in the visible light region (491 and 617 nm) are attributed to the s1 excitation state of S_6^{2-} (n $\rightarrow$ σ^* excitation) and the s3 excitation state of $S_3^{\bullet-}$ (n $\rightarrow$ π^* excitation), respectively. In the ultraviolet region, the absorption band at 355 nm is attributed to the two NTO pairs of S_6^{2-}, s5 and s8 (n $\rightarrow$ σ^* excitation). Both the s9 excitation state of $S_3^{\bullet-}$ and the s18 excitation state of S_6^{2-} contribute to the absorption band at 267 nm with n $\rightarrow$ σ^* excitation.

S5 Calculated UV-vis spectrum of $S_2^{\bullet-}$

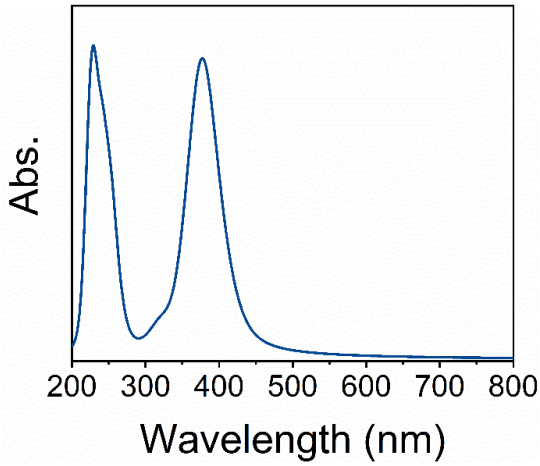

Fig. S6. Calculated UV-Vis spectrum of $S_2^{\bullet-}$, performed by the TD-DFT method[4] at M06-2X/6-311+G(2d,p) level of theory with the SMD solvation mode.

S6 The color of DMSO solution with different Li_2S_6 concentrations

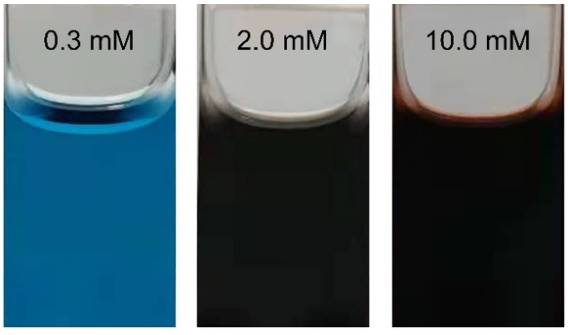

Fig. S7. The visible color change of DMSO solutions when Li_2S_6 was added at different concentrations. The solution was blue when $S_3^{\bullet-}$ was at a low concentration (0.3 mM), and it changed to red color with a higher concentration of S_6^{2-} (10.0 mM). The color changes imply that the entropy-driven dissociation reaction of S_6^{2-} into $S_3^{\bullet-}$ is also affected by the concentration of Li_2S_6.

S7 The UV-vis and ESR spectra of Li_2S_6 in Tetramethylurea solvent.

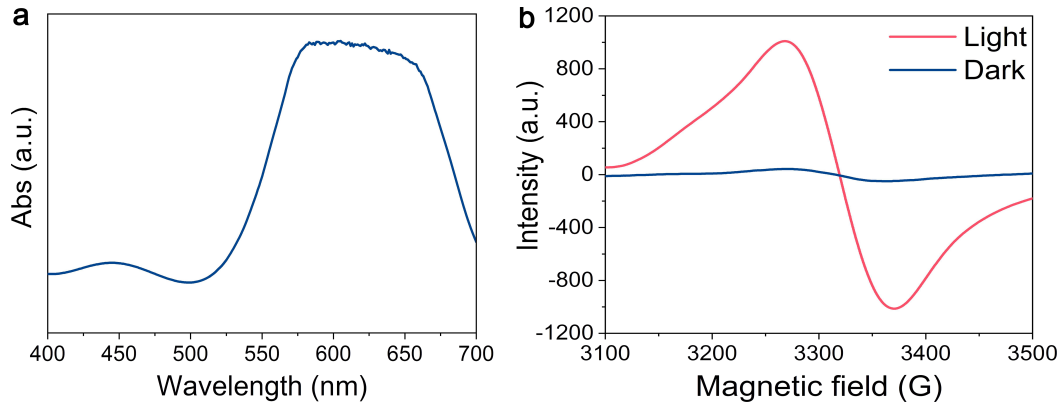

Fig. S8. Experimental test for highly solvating tetramethylurea solution of Li_2S_6. (a) UV-vis spectrum; (b) ESR spectra under light and dark

S8 The cyclic performance of Li–S batteries with and without pre-introducing $S_3^{\bullet-}$

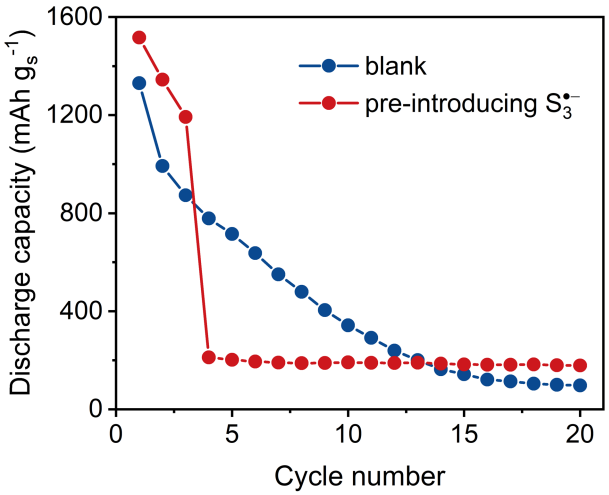

Fig. S9. The cycling performance of Li–S batteries with (blank) and without pre-introducing $S_3^{\bullet-}$.

Fig. S9 shows that the Li–S battery with pre-introducing $S_3^{\bullet-}$ has a higher discharge capacity, compared with the blank one during the first 3 cycles, suggesting that $S_3^{\bullet-}$ can enhance sulfur utilization in the electrochemical reactions. However, the higher sulfur utilization also leads to more dissolution of polysulfides. So, the Li–S battery with pre-introducing $S_3^{\bullet-}$ shows a quickly capacity decay, resulting from the more severe shuttle.

S9 SEM images of anode retrieved from the blank cells and the cells of adding 5 mM Li_2S_6

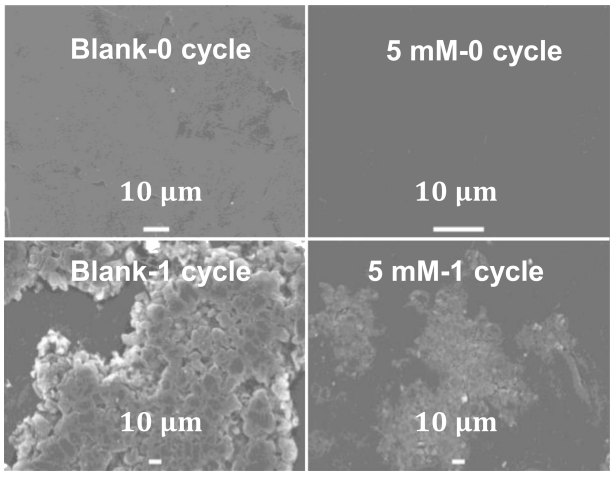

Fig. S10. SEM images of anode retrieved from the blank cells and the cells of adding 5 mM Li_2S_6.

References

1. Y. Zhao and D. G. Truhlar, *J. Chem. Phys.*, 2006, **125**, 194101.
2. J. R. Pliego and J. M. Riveros, *J. Phys. Chem. A*, 2001, **105**, 7241-7247.
3. A. V. Marenich, C. J. Cramer and D. G. Truhlar, *J. Phys. Chem. B*, 2009, **113**, 6378-6396.
4. X. Li, N. Govind, C. Isborn, A. E. DePrince and K. Lopata, *Chem. Rev.*, 2020, **120**, 9951-9993.
5. M. Isegawa, R. Peverati and D. G. Truhlar, *J Chem. Phys.*, 2012, **137**, 244104.
6. L. R. Domingo, E. Chamorro and P. Pérez, *J. Org. Chem.*, 2008, **73**, 4615-4624.
7. M. J. Frisch, G. W. Trucks, H. B. Schlegel, G. E. Scuseria, M. A. Robb, J. R. Cheeseman, G. Scalmani, V. Barone, G. A. Petersson, H. Nakatsuji, X. Li, M. Caricato, A. V. Marenich, J. Bloino, B. G. Janesko, R. Gomperts, B. Mennucci, H. P. Hratchian, J. V. Ortiz, A. F. Izmaylov, J. L. Sonnenberg, Williams, F. Ding, F. Lipparini, F. Egidi, J. Goings, B. Peng, A. Petrone, T. Henderson, D. Ranasinghe, V. G. Zakrzewski, J. Gao, N. Rega, G. Zheng, W. Liang, M. Hada, M. Ehara, K. Toyota, R. Fukuda, J. Hasegawa, M. Ishida, T. Nakajima, Y. Honda, O. Kitao, H. Nakai, T. Vreven, K. Throssell, J. A. Montgomery Jr., J. E. Peralta, F. Ogliaro, M. J. Bearpark, J. J. Heyd, E. N. Brothers, K. N. Kudin, V. N. Staroverov, T. A. Keith, R. Kobayashi, J. Normand, K. Raghavachari, A. P. Rendell, J. C. Burant, S. S. Iyengar, J. Tomasi, M. Cossi, J. M. Millam, M. Klene, C. Adamo, R. Cammi, J. W. Ochterski, R. L. Martin, K. Morokuma, O. Farkas, J. B. Foresman and D. J. Fox, *Gaussian 16, Revision B.01, Gaussian, Inc., Wallingford CT, 2016.*
8. W. M. Haynes, *CRC handbook of chemistry and physics*, CRC press, 2014.
9. Y. Zhao and D. G. Truhlar, *Theor. Chem. Acc.*, 2008, **120**, 215-241.
10. S. Grimme, J. Antony, S. Ehrlich and H. Krieg, *J. Chem. Phys.*, 2010, **132**, 154104.
11. E. Westphal and J. R. Pliego, *J. Chem. Phys.*, 2005, **123**, 074508.
12. R. L. Martin, *J. Chem. Phys.*, 2003, **118**, 4775-4777.